**Aalborg Universitet**

AALBORG UNIVERSITY

DENMARK

# Control Strategies for Islanded Microgrid using Enhanced Hierarchical Control Structure with Multiple Current-Loop Damping Schemes

Han, Yang; Shen, Pan; Zhao, Xin; Guerrero, Josep M.

# Control Strategies for Islanded Microgrid using Enhanced Hierarchical Control Structure with Multiple Current-Loop Damping Schemes

Yang Han, *Member, IEEE*, Pan Shen, Xin Zhao, and Josep M. Guerrero, *Fellow, IEEE*

*Abstract*—In this paper, the modeling, controller design, and stability analysis of the islanded microgrid (MG) using enhanced hierarchical control structure with multiple current loop damping schemes is proposed. The islanded MG is consisted of the parallel-connected voltage source inverters using LCL output filters, and the proposed control structure includes: the primary control with additional phase-shift loop, the secondary control for voltage amplitude and frequency restoration, the virtual impedance loops which contains virtual positive- and negative-sequence impedance loops at fundamental frequency, and virtual variable harmonic impedance loop at harmonic frequencies, and the inner voltage and current loop controllers. A small-signal model for the primary and secondary controls with additional phase-shift loop is presented, which shows an over-damped feature from eigenvalue analysis of the state matrix. The moving average filter-based sequence decomposition method is proposed to extract the fundamental positive and negative sequences, and harmonic components. The multiple inner current loop damping scheme is presented, including the virtual positive, virtual negative and variable harmonic sequence impedance loops for reactive and harmonic power sharing purposes and the proposed active damping scheme using capacitor current feedback loop of the LCL-filter, which shows enhanced damping characteristics and improved inner-loop stability. Finally, the experimental results are provided to validate the feasibility of the proposed approach.

Y. Han and P. Shen are with the Department of Power Electronics, School of Mechatronics Engineering, University of Electronic Science and Technology of China, No.2006, Xiyuan Avenue, West Hi-Tech Zone, Chengdu 611731, China (e-mail: hanyang@uestc.edu.cn; panshen01@126.com), also with the State Key Laboratory of Power Transmission Equipment & System Security and New Technology, Chongqing University, Chongqing 400044, China, and also with Artificial Intelligence Key Laboratory of Sichuan Province, Sichuan University of Science and Engineering, Zigong 643000, China.

X. Zhao and J. M. Guerrero are with the Department of Energy Technology, Aalborg University, Aalborg 9220, Denmark (e-mail: xzh@et.aau.dk, joz@et.aau.dk).

*Index Terms*—Microgrid, droop control, secondary control, phase-shift control, small-signal model, power sharing, virtual impedance, active damping, voltage control.

## Nomenclature

| | |
|---|---|
| DG | Distributed generator. |
| MG | Microgrid. |
| VSI | Voltage source inverter. |
| AD | Active damping. |
| THD | Total harmonic distortion. |
| PV | Photovoltaic cell. |
| ESS | Energy storage system. |
| SoC | State of charge. |
| APF | Active power filter. |
| LPF | Low-pass filter. |
| PLL | Phase locked loop. |
| $P, Q$ | Active and reactive output powers. |
| $\omega, E$ | Angular frequency and amplitude of the output voltage references. |
| $p, q$ | Instantaneous active and reactive powers. |
| $v_{C\alpha}, v_{C\beta}$ | $\alpha\beta$-axis output voltage. |
| $i_{o\alpha}, i_{o\beta}$ | $\alpha\beta$-axis output current. |
| $\omega_c$ | Cut-off frequency of the LPF. |
| $k_{pf}, k_{if}$ | Parameters of the frequency restoration control. |
| $k_{pe}, k_{ie}$ | Parameters of the voltage restoration control. |
| $\omega_{MG}, E_{MG}$ | Angular frequency and voltage amplitude of MG. |
| $\omega_{sec}, E_{sec}$ | Angular frequency and voltage amplitude of the restoration controller. |
| $\tau$ | PLL time constant. |
| $k_d$ | Additional phase-shift coefficient. |
| $\delta$ | The phase angle of the MG system. |
| $\delta_d$ | The phase angle displacement of the additional phase-shift loop. |
| $\delta_p$ | The phase angle of the power-frequency droop controller. |
| $k_p, k_q$ | Frequency and voltage droop coefficients. |
| $\Delta$ | Small deviation of the variable. |
| $T_\omega$ | Window length of the moving average filter. |
| $Z_{v\alpha\beta}$ | Resistive-inductive virtual impedance of MG. |
| $Z_{o\alpha\beta}$ | Output impedance of MG. |
| $v_{dc}$ | DC voltage of MG. |
| $\omega_0, f_s$ | Fundamental and switching frequencies. |
| $L, L_o$ | Filter and output inductances. |

| $C$ | Filter capacitor. |
|---|---|
| $R_L$ | Balanced resistive load. |
| $L_{NL}, R_{NL}, C_{NL}$ | Nonlinear load parameters. |
| $k_{AD}$ | Active damping coefficient. |
| $k_{pv}, k_{rv}, k_{hv}$ | Parameters of the voltage controller. |
| $k_{pi}, k_{ri}, k_{hi}$ | Parameters of the current controller. |

## I. INTRODUCTION

RECENTLY, distributed generators (DGs) based on renewable energy, such as solar power plants, and wind turbines, etc., are attracting more and more attention for their environmental friendly characteristics [1]. High penetration levels of DGs may cause inverse power flow, voltage fluctuation, and other problems in distribution systems. Microgrids (MGs), which contain a number of systematically organized DG units, have been emerging as a framework to overcome the problems caused by the high levels of penetration of DG and make large-scale application of DG possible [2]. As an interface between the DG and the power grid or local loads, a voltage source inverter (VSI) is the most common topology which can operate either in grid-connected or islanded mode to provide a controlled and high-quality power exchange with the grid or local loads.

In islanded mode, the local loads should be supplied by the DG units, which now act as controlled voltage sources (CVS) [3]. And the MGs need some form of control in order to avoid circulating currents between the DG units and ensure stable and efficient operation. The important roles that can be achieved using these control structures are active and reactive power control capabilities among the DGs, energy management, frequency and voltage regulation, and economic optimization [4]. Many control strategies of parallel VSIs forming an MG have been investigated [5-9], where the decentralized and cooperative controllers such as the droop methods have been proposed and are considered as preferred option due to several attractive advantages such as flexibility, and no need of high bandwidth communications [10]. The droop control is a kind of cooperative control that allows parallel connection of VSIs sharing active and reactive powers [11]. In order to analyze the performance of these methods, recent literature addressing the stability and dynamic performance of the droop-controlled MGs by using state-space and small-signal models have been presented [8], [12]. The virtual impedance can be added in the control loop to enhance the reliability and performance of the droop-controlled VSIs, ensuring the inductive behavior of the output impedance of the DGs. The transients during fast load switching and voltage quality under nonlinear loads in MG may also be influenced by virtual impedance effects [7], [9], [13].

It is reported in [14] that the droop control methods involve an inherent trade-off between power sharing and voltage and frequency regulation. The secondary controllers were proposed to compensate the deviations of voltage and frequency in [4], [5], [15]. The islanded MGs can restore the frequency and voltage amplitude in spite of deviations created by the total amount of active and reactive powers demanded by the loads [15] while the influence of this secondary control on the stability and dynamic performance of MG was not considered.

The increasing proliferation of nonlinear loads could result in significant harmonic distortion in the distribution systems. And a MG should be able to operate under nonlinear load conditions without performance degradations. Based on the IEEE standard 519-1992 [16], the voltage total harmonic distortion (THD) for sensitive loads should be maintained below 5%. In industrial applications, LC filters are usually used as an interface between the inverter and the local loads to effectively mitigate the harmonic contents of the inverter output waveforms [17]. The pure LC or LCL circuits are highly susceptible to resonances with harmonic components generated by the inverter or the distorted nonlinear loads. In order to mitigate system resonances, a damping resistor can be placed in the LC or LCL circuit, but results in power loss [18]. To avoid drawbacks of passive damping, various active damping (AD) methods based on the inner loop feedback variables have been developed [19], [20]. Among AD methods, the method involving feedback of the capacitor current of the LCL filter has attracted attention due to its effectiveness, simple implementation, and wide application [20].

The various hierarchical control strategies for MGs have been presented in our previous works [21-26], where the power oscillations, accuracy of the droop control, and the power sharing problems are seldom considered. In [21], the parallel-connected bidirectional converters for AC and DC hybrid MG application are analyzed in standalone operation mode and the conventional hierarchical control in stationary frame under resistive conditions is adopted. A general approach of hierarchical control for MG is presented in [22], the tertiary control could provide high-level inertias to interconnect more MGs, acting as the primary control of the cluster and the tertiary cluster control can fix the active and reactive powers to be provided by this cluster or act like a primary control to interconnect more MG clusters. In another hierarchical control structure, an autonomous active power control strategy is modeled for MGs with photovoltaic cell (PV) generation, energy storage system (ESS) and loads to achieve power management in a decentralized manner [23], and the state of charge (SoC) of the ESS can be kept within the safe limits by automatically adjusting the power generation from the PV systems and load consumption. In [24], the coordinated control of DG inverter and active power filter (APF) to compensate voltage harmonics in MG is addressed, the APF participates in harmonic compensation and consequently the compensation efforts of DG decrease to avoid excessive harmonics or loading of the DG inverter. In [25], the advanced decentralized and hierarchical control methods are reviewed, and future trends in hierarchical control for MGs and the clusters of MGs are given.

In this paper, the enhanced hierarchical control for islanded MG is presented, using multiple inner loop active damping schemes, which shows improved characteristics in terms of hierarchical control structure including the droop control with additional phase-shift loop and the centralized secondary control scheme for voltage amplitude and frequency restoration purposes of MG. A small signal model is developed for the power control loop, which takes the droop control with additional phase-shift loop and secondary control into consideration. The power control loop is designed to be overdamped to suppress power oscillations. The proposed multiple active damping and virtual impedance schemes are

adopted for the inner loops, i.e., the capacitor current feedback loop plus the output virtual impedance loops, which achieves the purposes of inverter side LC resonance active damping, reactive power and harmonic power sharing.

The proposed approach employs the moving average filter-based sequence decomposition which is composed of the virtual positive- and negative-sequence impedance loops at fundamental frequency, and the virtual variable harmonic impedance loop at harmonic frequencies [27], [28]. The virtual positive- and negative-sequence impedance loops improve the performance of the active power-frequency (P-ω) and reactive power-voltage magnitude (Q-E) droop controllers and reduce the fundamental negative sequence circulating current. A proper sharing of harmonic power among all the DG inverters is achieved by using the virtual variable harmonic impedance loop at characteristic harmonic frequencies. The feasibility of the proposed approach is validated by the experimental results obtained from two parallel-connected 2.2kW Danfoss inverters under linear and nonlinear load conditions. The main novelties in this paper are listed below.

1) Development of the accurate small-signal model of the power controller and integration with the secondary controller. A state equation model of the islanded MG is presented, using the primary and secondary controls, including an additional phase-shift loop for power oscillation damping.
2) Implementation of the virtual positive-sequence and negative-sequence impedance loops at fundamental frequency, and the virtual variable harmonic impedance loop at harmonic frequencies for reactive and harmonic power sharing among the DG inverters. The moving average filter-based sequence decomposition method is proposed to extract the fundamental positive- and negative-sequence, and harmonic components.
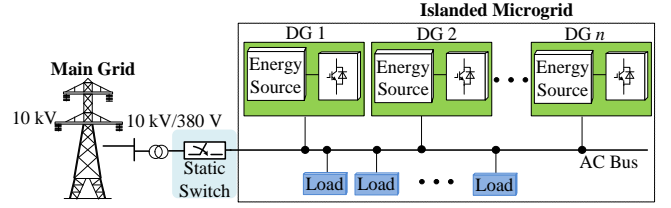


Fig. 1. Typical structure of MG with DGs and multiple loads.

3) Development of the AD strategy for resonance damping of the islanded MG. The multiple inner loop with AD strategy is proposed to avoid resonance and improve stability of the inner loop controller of the enhanced hierarchical structure of the islanded MG system.

The remainder of this paper is structured as follows. The enhanced hierarchical control structure and strategy of the islanded MG system are analyzed in detail in Section II, including the droop control, secondary control, small-signal analysis of the power controller, virtual impedance loop, inner voltage and current control loops. Section III provides comprehensive experimental results. Finally, Section IV concludes this paper.

## II. ENHANCED HIERARCHICAL CONTROL STRATEGY

A typical structure of MG with *n* DGs and loads is given in Fig. 1. Although the proposed control strategies can operate in either the grid-connected mode or islanded mode, only the islanded operation mode will be considered in this paper. The three-phase VSIs with LCL filters are usually used as the DG interfaces to connect with the local AC bus, and the power stage of two DGs and the proposed control strategy for their interface inverters connected in an islanded mode are shown in Fig. 2. Each DG unit with its LCL filter can be considered as a subsystem of the MG.
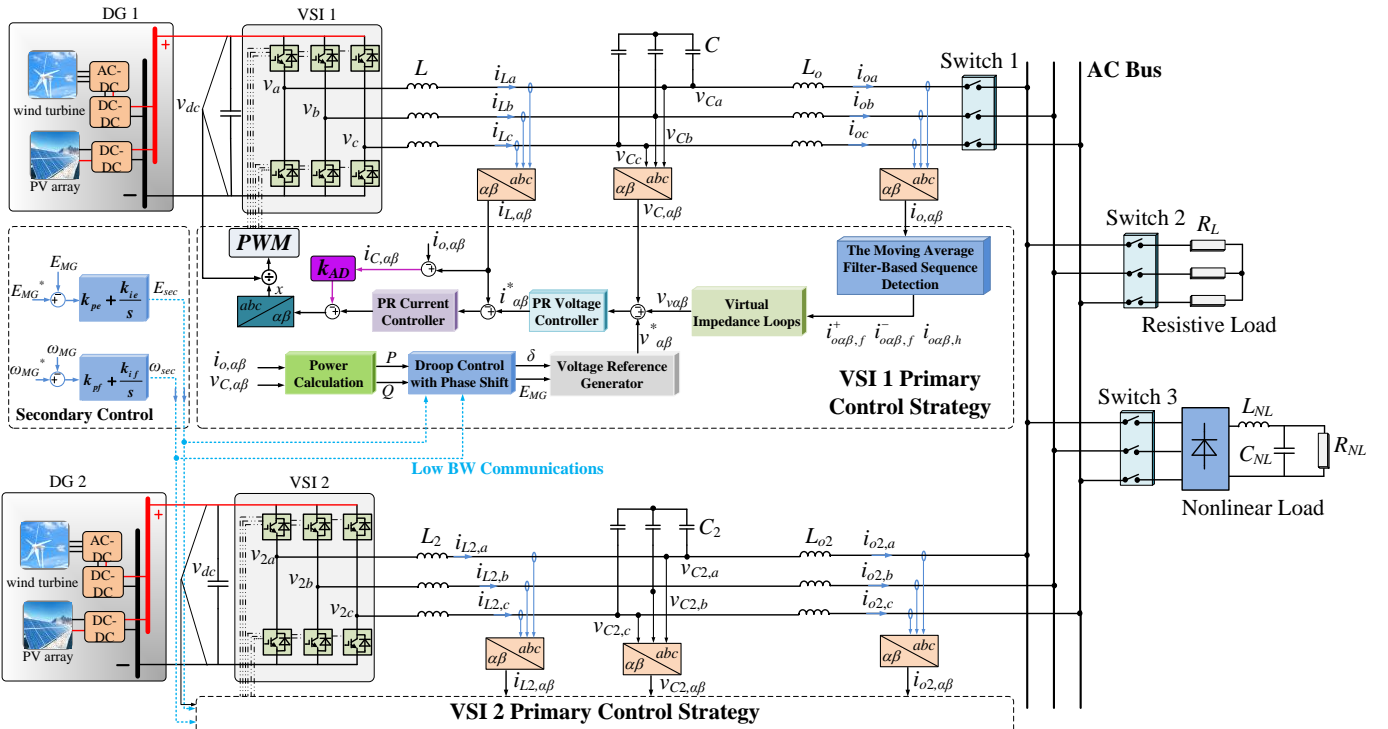


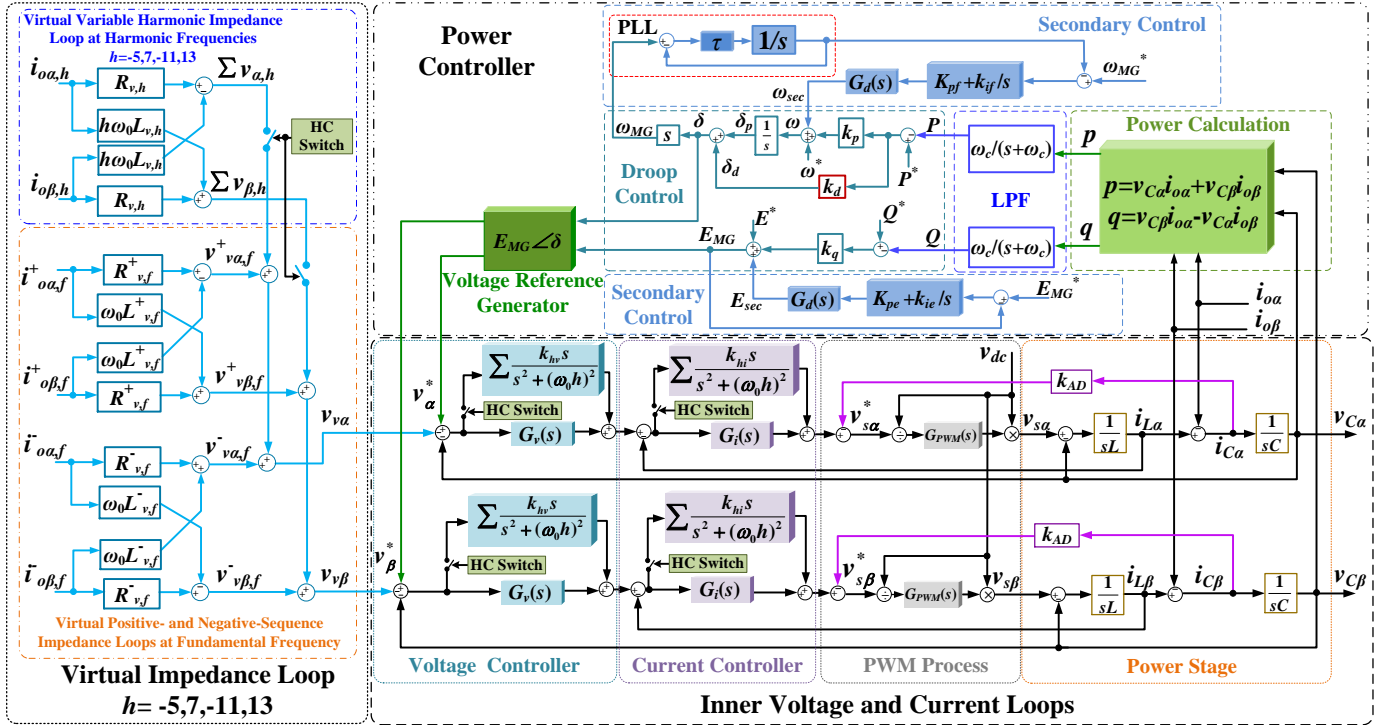Fig. 2. MG power stage and control system.

Fig. 3. Block diagram of the proposed enhanced hierarchical control strategy with multiple inner-loop damping schemes.

As shown in Fig. 3, the control strategy of an individual DG unit is implemented in the stationary reference frame. The dynamics of the DG units are influenced by the output LCL filter, the droop controller, the secondary controller with frequency and voltage amplitude restoration, the power calculation, the virtual impedance loops which contain the virtual positive- and negative-sequence impedance loops at fundamental frequency, and the virtual variable harmonic impedance loop at harmonic frequencies, and the PR-based inner voltage and current loops. The proposed control strategies are presented as follows.

*A. Droop Control for MGs*

The droop control is utilized to avoid communication wires while obtaining good power sharing, which is responsible for adjusting the frequency and amplitude of the voltage reference according to the active and reactive powers ($P$ and $Q$), ensuring $P$ and $Q$ flow control [11], [13]. The active power frequency ($P$-$\omega$) and reactive power voltage magnitude ($Q$-$E$) droop control schemes are defined as

$$\omega = \omega^* - k_p(P - P^*) , \quad E = E^* - k_q(Q - Q^*) \qquad (1)$$

where $\omega$ and $E$ represent the frequency and amplitude of the output voltage references, $\omega^*$ and $E^*$ are the nominal frequency and amplitude, $P^*$ and $Q^*$ are the active and reactive power references normally set to zero in islanded MG [26], [29], and $k_p$ and $k_q$ are the droop coefficients.

Referring to [11], the instantaneous active power ($p$) and reactive power ($q$) are calculated from the $\alpha\beta$-axis output voltage ($v_{C\alpha\beta}$) and current ($i_{o\alpha\beta}$) as

$$p = v_{C\alpha}i_{o\alpha} + v_{C\beta}i_{o\beta}, \quad q = v_{C\beta}i_{o\alpha} - v_{C\alpha}i_{o\beta} \qquad (2)$$

The instantaneous powers are then passed through low-pass filters with the cut-off frequency $\omega_c$ to obtain the filtered output real and reactive powers ($P$ and $Q$) as follows

$$P = \frac{\omega_c}{s + \omega_c} p , \quad Q = \frac{\omega_c}{s + \omega_c} q \qquad (3)$$

The bandwidth of the low pass filter is much smaller than that of the inner controllers of DG unit and the performance of the system is strongly influenced by this fact [8].

*B. The Secondary Control for MGs*

The inherent trade-off between power sharing and voltage and frequency regulation is one drawback of the droop method. The conventional droop control is local and does not have communications with other DG units. In order to mitigate these disadvantages, a restoration control can be added to remove any steady-state error introduced by the conventional droop and achieve global controllability of the MG that ensures nominal values of voltage and frequency in the MG [4], [5], [11]. As shown in Fig. 2, the primary and secondary controls are implemented in each DG unit. The secondary control is realized by low bandwidth communication among the DG units. By using this approach, the frequency and voltage amplitude restoration compensators can be derived as [4]

$$\begin{cases} \omega_{sec} = k_{pf}(\omega_{MG}^* - \omega_{MG}) + k_{if} \int (\omega_{MG}^* - \omega_{MG})dt \\ E_{sec} = k_{pe}(E_{MG}^* - E_{MG}) + k_{ie} \int (E_{MG}^* - E_{MG})dt \end{cases} \qquad (4)$$

where $k_{pf}$, $k_{if}$, $k_{pe}$, and $k_{ie}$ are the control parameters of the proportional integral (PI) compensator of the frequency and voltage restoration control, respectively. The angular frequency level in the MG ($\omega_{MG}$) are measured and compared to the reference ($\omega_{MG}^*$) and the errors processed by the PI compensator are sent to all the DGs in order to restore the frequency of MG. The control signal ($E_{sec}$) is sent to primary control level of each DG in order to remove steady-state errors of the droop control.

*1) Frequency control*: Taking the idea from large electrical power systems, in order to compensate the frequency deviation

produced by the local $P$-$\omega$ droop controllers, secondary frequency controllers have been proposed in [11]. A model of the frequency secondary control is shown in Fig. 4, which is also depicted in Fig. 3 in detail.
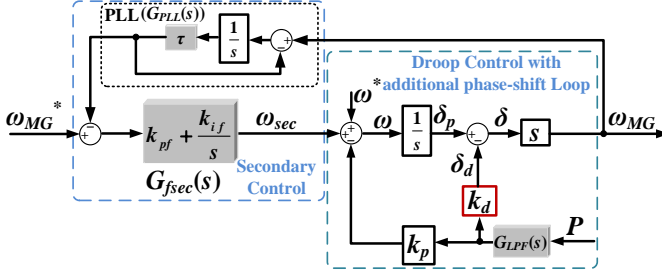


Fig. 4. Block diagram of frequency control for a DG unit.
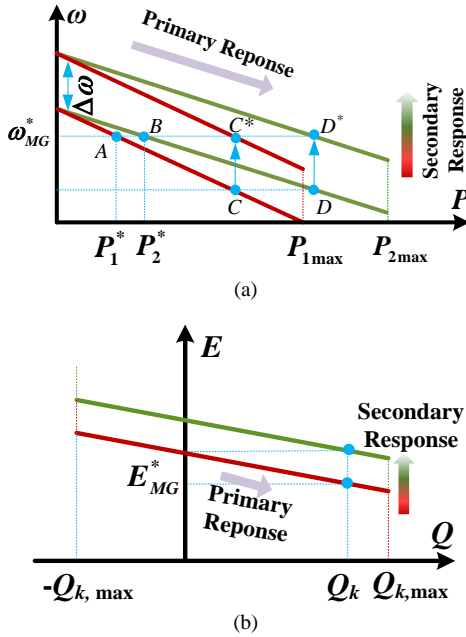


(a)



(b)

Fig. 5. Secondary control versus primary control response. (a) Frequency restoration. (b) Voltage amplitude restoration.

The control block diagram in Fig. 4 includes the droop control and secondary control. For droop control model, a low-pass filter ($G_{LPF}$ $(s)$) with cutting frequency of 5 Hz has been considered for power calculation. The secondary control has been modeled by means of a simplified PLL first-order transfer function ($G_{PLL}(s)$) with the gain ($\tau$) used to extract the frequency of the MG, the secondary PI controller ($G_{fsec}(s)$) is used to restore the frequency deviations [11], and a proportional gain ($k_d$) of the additional phase-shift loop is super-imposed to the active power control loop to suppress power oscillation [8]. The additional phase-shift loop performs a phase displacement $\delta_d$ which is added to the phase determined by the $P$-$\omega$ droop $\delta_p$, resulting in the angle $\delta$ of the inverter voltage $E_{MG}$. This strategy increases system damping, and the phase of inverter $\delta$ which is used by the reference generator block, is calculated by

$$\delta = \delta_p + \delta_d \quad (5)$$

From the block diagram of Fig. 4, $\omega_{MG}$ is derived as

$$\omega_{MG} = \frac{G_{f\,sec}(s)}{1+G_{f\,sec}(s)G_{PLL}(s)}\omega_{MG}^* - \frac{(k_p+sk_d)G_{LPF}(s)}{1+G_{f\,sec}(s)G_{PLL}(s)}P \quad (6)$$

where $G_{LPF}(s)$, $G_{fsec}(s)$ and $G_{PLL}(s)$ are expressed as

$$G_{LPF}(s) = \frac{\omega_c}{s+\omega_c} , \; G_{f\,sec}(s) = k_{pf} + \frac{k_{if}}{s} , \; G_{PLL}(s) = \frac{1}{\tau s+1} \quad (7)$$

Fig. 5 shows the operation principle of secondary control, which removes frequency and voltage amplitude deviations caused by the primary control loop [5]. The characteristic of secondary control for the frequency restoration is shown in Fig. 5(a). It can be seen that secondary control shifts up the primary response so that frequency reaches to the nominal value. As shown in Fig. 5(a), the points of $A$ and $B$ are the nominal frequencies of the DG1 and DG2, respectively. The operation points of DG1 and DG2 deviate from the nominal frequencies and operate at the points of $C$ and $D$ when a transient increase of load is applied in the system. The idling frequency changes and the operation points of DG1 and DG2 shift to new operating points of $C^*$ and $D^*$ after the secondary controller is applied in the control system. Without this action, the frequency of the MG is load dependent.
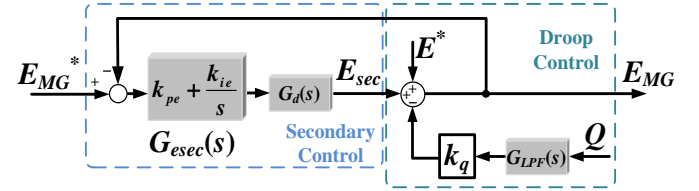


Fig. 6. Block diagram of voltage amplitude control for a DG unit.

*2) Voltage control*: A similar approach can be used as in the frequency secondary control, in which each DG unit measures the voltage error, and tries to compensate the voltage deviation caused by the $Q$-$E$ droop [4], [11]. As shown in Fig. 5(b), the secondary control is able to remove voltage deviations caused by primary control in DG unit and the voltage amplitude restoration can be achieved. Fig. 6 shows the simplified control diagram in this case. The closed-loop voltage dynamic model can be obtained as

$$E_{MG} = \frac{G_{e\,sec}(s)G_d(s)}{1+G_{e\,sec}(s)}E_{MG}^* - \frac{k_qG_{LPF}(s)}{1+G_{e\,sec}(s)}Q , \; G_{e\,sec}(s) = k_{pe}+\frac{k_{ie}}{s} \quad (8)$$

### C. Small-Signal Analysis of the Power Controller

This section presents the small-signal model of the primary and secondary controllers with additional phase-shift loop, emphasizing stability of the MG power controller. The small-signal dynamics of the restoration control can be obtained by linearizing (4)

$$\Delta\omega_{sec} = -k_{pf}\Delta\omega_{MG} - \frac{k_{if}}{s}\Delta\omega_{MG} , \; \Delta E_{sec} = -k_{pe}\Delta E_{MG} - \frac{k_{ie}}{s}\Delta E_{MG} \quad (9)$$

where the symbol $\Delta$ in (9) denotes the small deviation of the variable from the equilibrium point [8].

Taking (1)-(5) into account, the droop control with centralized secondary restoration control can be obtained as

$$\omega = \omega_{sec} + \omega^* - k_p(P-P^*) , \; E_{MG} = E_{sec} + E_{MG}^* - k_q(Q-Q^*) \quad (10)$$

By linearizing (10), and substituting (9) for (10), the small-signal model can be written as

$$\begin{cases} \Delta\omega = -k_{pf}\Delta\omega_{MG} - \dfrac{k_{if}}{s}\Delta\omega_{MG} - k_p\Delta P \\[2mm] \Delta E_{MG} = -k_{pe}\Delta E_{MG} - \dfrac{k_{ie}}{s}\Delta E_{MG} - k_q\Delta Q \end{cases} \quad (11)$$

The linearized small-signal models of $P$ and $Q$ can be written as

$$\begin{cases} \Delta \dot{P} = -\omega_c \Delta P + \omega_c (I_{o\alpha} \Delta v_{C\alpha} + I_{o\beta} \Delta v_{C\beta} + V_{C\alpha} \Delta i_{o\alpha} + V_{C\beta} \Delta i_{o\beta}) \\ \Delta \dot{Q} = -\omega_c \Delta Q + \omega_c (I_{o\alpha} \Delta v_{C\beta} - I_{o\beta} \Delta v_{C\alpha} + V_{C\beta} \Delta i_{o\alpha} - V_{C\alpha} \Delta i_{o\beta}) \end{cases} \quad (12)$$
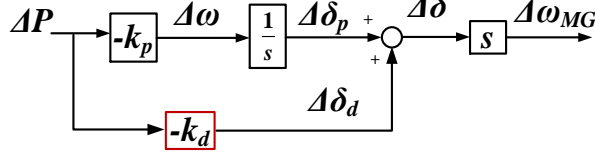


Fig. 7. Linearized model of the additional phase-shift loop for $P$-$\omega$ droop control.

Fig. 7 shows the linearized model for frequency and power angle loop, and the linearized inverter phase angle is given by

$$\Delta \delta = \Delta \delta_p + \Delta \delta_d = \frac{1}{s} \Delta \omega - k_d \Delta P \quad (13)$$

Substituting $\Delta \omega$ of (11) for (13), we get

$$s \Delta \delta = -k_{pf} \Delta \omega_{MG} - \frac{k_{if}}{s} \Delta \omega_{MG} - k_p \Delta P - s k_d \Delta P \quad (14)$$

At this point, as shown in Fig. 7, note that the first derivative of the inverter phase angle ($d\delta/dt$) is not the droop frequency ($\omega$) but the MG frequency ($\omega_{MG}$) and the first state variables for the state equation model can be obtained as

$$\Delta \dot{\delta}(t) = \Delta \omega_{MG}(t) \quad \text{or} \quad s \Delta \delta(s) = \Delta \omega_{MG}(s) \quad (15)$$

Considering that the frequency is the first-order derivative of the phase angle, we get

$$s \Delta \delta = s \Delta \delta_p + s \Delta \delta_d = \Delta \omega_{MG} = \Delta \omega + \Delta \omega_d \quad (16)$$

Based on (11), (13), and (16), the equations that relates the frequency shift and secondary control of the inverter can be calculated due to the active power deviation from the equilibrium point, thus we get

$$(1+k_{pf}) \Delta \dot{\omega}_{MG} = -k_{if} \Delta \omega_{MG} - (k_p + k_d) \Delta \dot{P} \quad (17)$$

Finally, according to $\Delta E_{MG}$ of (11), the derivative of $E_{MG}$ can be obtained as

$$(1+k_{pe}) \Delta \dot{E}_{MG} = -k_{ie} \Delta E_{MG} - k_q \Delta \dot{Q} \quad (18)$$

By rearranging (9)-(18), the small-signal power controller model can be written in a state-space form as in (19), which describes the behavior of the states $\Delta\delta$, $\Delta\omega_{MG}$, $\Delta E_{MG}$ and $\Delta P$, and $\Delta Q$ on the $k$-th ($k$=1, 2) inverter in function of the deviations of the active power and reactive power from the equilibrium point.

$$\begin{bmatrix} \Delta \dot{\delta}_k \\ \Delta \dot{\omega}_{MGk} \\ \Delta \dot{E}_{MGk} \\ \Delta \dot{P}_k \\ \Delta \dot{Q}_k \end{bmatrix} = \mathbf{M_k} \begin{bmatrix} \Delta \delta_k \\ \Delta \omega_{MGk} \\ \Delta E_{MGk} \\ \Delta P_k \\ \Delta Q_k \end{bmatrix} + \mathbf{N_k} \begin{bmatrix} \Delta v_{C\alpha\beta k} \\ \Delta i_{o\alpha\beta k} \end{bmatrix} \quad (19)$$

Or symbolically, represented as

$$\left[ \Delta \dot{X}_k \right] = \mathbf{M_k} \left[ \Delta X_k \right] + \mathbf{N_k} \left[ \Delta S_k \right] \quad (20)$$

where $\mathbf{M_k}$ and $\mathbf{N_k}$ are derived as

$$\mathbf{M_k} = \begin{bmatrix} 0 & 1 & 0 & 0 & 0 \\ 0 & \dfrac{-k_{if}}{1+k_{pf}} & 0 & 0 & 0 \\ 0 & 0 & \dfrac{-k_{ie}}{1+k_{pe}} & 0 & \dfrac{-k_q\omega_c}{1+k_{pe}} \\ 0 & 0 & 0 & -\omega_c & 0 \\ 0 & 0 & 0 & 0 & -\omega_c \end{bmatrix},$$

$$\mathbf{N_k} = \begin{bmatrix} 0 & 0 & 0 & 0 \\ \eta I_{o\alpha k} & \eta I_{o\beta k} & \eta V_{C\alpha k} & \eta V_{C\beta k} \\ -\gamma I_{o\alpha k} & \gamma I_{o\beta k} & -\gamma V_{C\alpha k} & \gamma V_{C\beta k} \\ \omega_c I_{o\alpha k} & \omega_c I_{o\beta k} & \omega_c V_{C\alpha k} & \omega_c V_{C\beta k} \\ \omega_c I_{o\alpha k} & -\omega_c I_{o\beta k} & \omega_c V_{C\beta k} & -\omega_c V_{C\alpha k} \end{bmatrix} \quad (21)$$

with

$$\eta = \frac{-(k_p + k_d)\omega_c}{1+k_{pf}} \quad , \quad \gamma = \frac{k_q\omega_c}{1+k_{pe}} \quad . \quad (22)$$

Taking the Laplace transformation on both sides of (20), using initial conditions of $x_{init}$=0, we get

$$s \left[ \Delta X_k(s) \right] = \mathbf{M_k} \left[ \Delta X_k(s) \right] + \mathbf{N_k} \left[ \Delta S_k(s) \right] \quad (23)$$

$$(s\mathbf{I}_{5\times5} - \mathbf{M_k})\left[ \Delta X_k(s) \right] = \mathbf{N_k} \left[ \Delta S_k(s) \right] \quad (24)$$

where $\mathbf{I}_{5\times5}$ is a fifth order identity matrix. Then, assuming $(s\mathbf{I}_{5\times5}-\mathbf{M_k})$ is nonsingular, $\Delta X_k(s)$ can be calculated as

$$\left[ \Delta X_k(s) \right] = (s\mathbf{I}_{5\times5} - \mathbf{M_k})^{-1} \mathbf{N_k} \left[ \Delta S_k(s) \right] \quad (25)$$

By using adjoint matrix $adj(s\mathbf{I}_{5\times5}$-$\mathbf{M_k})$, $\Delta X_k(s)$ can be rewritten as

$$\left[ \Delta X_k(s) \right] = \frac{adj(s\mathbf{I}_{5\times5}\text{ - }\mathbf{M_k})\mathbf{N_k} \left[ \Delta S_k(s) \right]}{\left| (s\mathbf{I}_{5\times5}\text{ - }\mathbf{M_k}) \right|} \quad (26)$$

To ensure system stable, the poles of the denominator of (26) must lies in the left-hand side of the $s$-plane, thus we get

$$D(s) = \left| (s\mathbf{I}_{5\times5}\text{ - }\mathbf{M_k}) \right| = 0 \quad (27)$$

TABLE I
THE PARAMETERS OF THE PRIMARY AND SECONDARY CONTROLLERS

| Symbol | Parameter | Value |
|---|---|---|
| $\omega_c$ | Measuring filter cut-off frequency | $10\pi$ rad/s |
| $k_p$, $k_q$ | Frequency and voltage droop coefficient | 0.0001 rad/s/W, 0.0001 V/Var |
| $k_{pf}$, $k_{if}$ | Frequency proportional and integral term of the secondary compensator | 0.8, 10 s$^{-1}$ |
| $k_{pe}$, $k_{ie}$ | Amplitude proportional and integral term of the secondary compensator | 0.8, 10 s$^{-1}$ |
| $k_d$ | Additional phase-shift coefficient | 0.000005 rad/W |
| $\tau$ | PLL time constant | 50 ms |
| $R_{v,f}$, $R_{v,5}$, $R_{v,7}$, $R_{v,11}$, and $R_{v,13}$ | Virtual resistances | 6, 1, 1, 1, and 1 $\Omega$ |
| $L_{v,f}$, $L_{v,5}$, $L_{v,7}$, $L_{v,11}$, and $L_{v,13}$ | Virtual inductances | 6, 2, 2, 1.5 and 1.5 mH |

Substituting parameters of Table I to (27), the eigenvalues of the matrix $\mathbf{M_k}$ defined by (21) are calculated as

$$\lambda_1 = 0, \ \lambda_2 = \lambda_3 = -5.5556, \ \lambda_4 = \lambda_5 = -31.4159. \quad (28)$$

Note that all the non-zero poles of the matrix $\mathbf{M_k}$ are real and the system is over-damped. According to [8], the calculation of $\delta$ derivative presents a high variation level due to the active power ripple, especially under nonlinear load conditions. $\omega$

instead of $\omega_{MG}$ is used as the frequency feedback for the secondary controller in the experiment.

### D. Virtual Impedance Loop

Virtual resistance enhances system damping without additional power loss, since it is provided by a control loop and it is possible to implement it without decreasing system efficiency [14]. When virtual inductance is utilized, the DG output impedance becomes more inductive, decreasing $P$ and $Q$ coupling, enhancing the system stability, and reducing power oscillations and circulating currents [4]. As shown in Fig. 3, the voltage drop across the virtual positive- and negative-sequence impedance, and the virtual variable harmonic impedance loops in $\alpha\beta$ reference frame are derived as

$$\begin{cases} v^+_{v\alpha,f}(s) = R^+_{v,f} i^+_{o\alpha,f} - \omega_0 L^+_{v,f} i^+_{o\beta,f} \\ v^+_{v\beta,f}(s) = R^+_{v,f} i^+_{o\beta,f} + \omega_0 L^+_{v,f} i^+_{o\alpha,f} \end{cases} \quad (29)$$

$$\begin{cases} v^-_{v\alpha,f}(s) = R^-_{v,f} i^-_{o\alpha,f} + \omega_0 L^-_{v,f} i^-_{o\beta,f} \\ v^-_{v\beta,f}(s) = R^-_{v,f} i^-_{o\beta,f} - \omega_0 L^-_{v,f} i^-_{o\alpha,f} \end{cases} \quad (30)$$

$$\begin{cases} v_{v\alpha,h}(s) = R_{v,h} i_{o\alpha,h} + h\omega_0 L_{v,h} i_{o\beta,h} \\ v_{v\beta,h}(s) = R_{v,h} i_{o\beta,h} - h\omega_0 L_{v,h} i_{o\alpha,h} \end{cases} \quad (31)$$

where $R^+_{v,f}$ and $L^+_{v,f}$ are the virtual fundamental frequency positive sequence resistance and inductance, $R^-_{v,f}$ and $L^-_{v,f}$ represent the virtual fundamental frequency negative sequence resistance and inductance, and $h$ denotes the dominant harmonic components, which are -5, 7, -11, 13, etc., and $\omega_0$ represents the system fundamental frequency.

At the fundamental frequency, the virtual positive sequence impedance loop is designed to be mainly inductive to improve the reactive power sharing based on the $Q$-$E$ droop [30]. And the problem of the presence of the high R/X ratio which causes a coupling in the control of active and reactive power when using the conventional droop controllers has been resolved. The virtual negative sequence impedance is designed to be resistive to minimize the negative sequence circulating current among the DGs [27]. And the size of negative inductance needs to be kept smaller than the effective inductance to guarantee the stability of the virtual variable harmonic impedance loop at harmonic frequencies, and the larger the positive resistance in the virtual variable harmonic impedance loop, the better the sharing of harmonic power can be achieved [31].

In order to extract the fundamental positive sequence and negative sequence currents as well as the dominant harmonic currents, a set of Park transformation and the moving average filters are presented for realizing the load current decomposition, which is shown in Fig. 8(a). The moving average filters are linear-phase finite impulse response filters that are easy to realize in practice, are cost effective in terms of the computational burden, and can act as ideal low-pass filters if certain conditions hold [28]. The transfer function of the moving average filter can be simply presented as

$$G_{MAF}(s) = \frac{1 - e^{-T_\omega s}}{T_\omega s} \quad (32)$$

where $T_\omega$ is referred to as the window length. The moving average filter passes the dc component, and completely blocks the frequency components of integer multiples of $1/T_\omega$ in hertz.
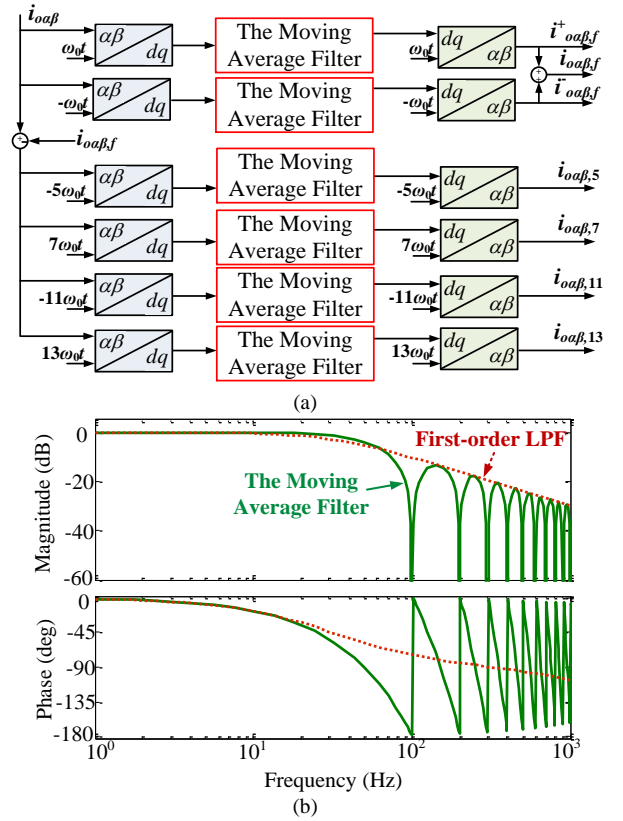


Fig. 8. The proposed moving average filter-based sequence decomposition of fundamental positive- and negative-sequence, and harmonic components. (a) Block diagram. (b) Bode plots for the moving average filter.

To provide a means of comparison, the transfer function of the first-order counterpart of the moving average filter is obtained as (33) by approximating the delay term in (32) by the first-order Padé approximation.

$$G_{MAF}(s)\Big|_{e^{-T_\omega s} \approx \frac{1 - T_\omega s/2}{1 + T_\omega s/2}} \approx \frac{1}{T_\omega s/2 + 1} \quad (33)$$

And the moving average filter with 0.01s window length ($T_\omega$) is used in the sequence decomposition and the bode plots of the moving average filter and the first-order LPF are shown in Fig. 8(b). It can be observed that, the moving average filter results in notches at the concerned harmonic frequencies. Consequently, the accuracy of the sequence decomposition is significantly improved by using the moving average filter.

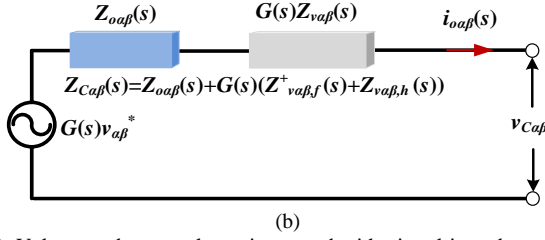### E. Inner Voltage and Current Control Loops



(a)
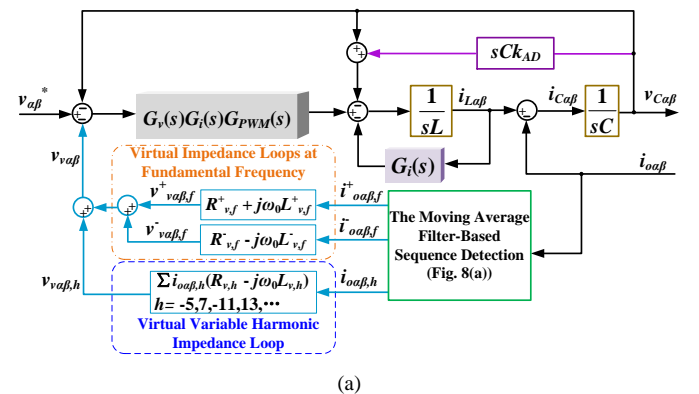
Fig. 9. Voltage and current loops integrated with virtual impedance loop. (a) Simplified model of the inner loops. (b) Equivalent impedance model of a VSI.

From system control diagram of Fig. 3, the simplified model of the inner loops is derived, as shown in Fig. 9(a). In order to overcome the drawbacks of the passive damping method, the active damping of a virtual resistor in parallel with the capacitor is used to avoid resonance and enhance stability of the inner loop controller.

The voltage loop reference signals are modified by the virtual impedance loop which contains the virtual positive- and negative-sequence impedance, and the virtual variable harmonic impedance loops are shown in Fig. 9(a). Then, the output voltage of the a DG unit can be derived as

$$v_{C\alpha\beta}(s) = G(s)v_{\alpha\beta}^{*} - (G(s)Z_{v\alpha\beta}(s) + Z_{o\alpha\beta}(s))i_{o\alpha\beta} \tag{34}$$

where $G(s)$, $Z_{v\alpha\beta}$, and $Z_{o\alpha\beta}$ are the closed-loop voltage transfer function, resistive-inductive virtual impedance, and the output impedance without virtual impedance loops, respectively [7], [13]. The virtual positive sequence impedance loop at fundamental frequency is only for attenuating circulating current, which can be omitted [27]. The transfer functions in (34) are derived as

$$G(s) = \frac{G_v(s)G_i(s)G_{PWM}(s)}{LCs^2 + (Cs + G_v(s))G_i(s)G_{PWM}(s) + k_{AD}Cs + 1} \tag{35}$$

$$Z_{v\alpha\beta}(s) = Z_{v\alpha\beta,f}^{+}(s) + Z_{v\alpha\beta,h}(s)$$
$$= \begin{bmatrix} R_{v,f}^{+} & -\omega_0 L_{v,f}^{+} \\ \omega_0 L_{v,f}^{+} & R_{v,f}^{+} \end{bmatrix} + \begin{bmatrix} R_{v,h} & h\omega_0 L_{v,h} \\ -h\omega_0 L_{v,h} & R_{v,h} \end{bmatrix} \tag{36}$$

$$Z_{o\alpha\beta}(s) = \frac{Ls + G_i(s)}{LCs^2 + (Cs + G_v(s) + k_{AD}Cs)G_i(s)G_{PWM}(s) + 1} \tag{37}$$

Under nonlinear load conditions, the dominant harmonic components should be taken into consideration for the voltage and current controllers in order to suppress output voltage harmonics. The transfer function of the voltage and current controllers are

$$G_v(s) = k_{pv} + \frac{k_{rv}s}{s^2 + \omega_0^2} + \sum_{h=-5,7,-11,13} \frac{k_{hv}s}{s^2 + (\omega_0 h)^2} \tag{38}$$

$$G_i(s) = k_{pi} + \frac{k_{ri}s}{s^2 + \omega_0^2} + \sum_{h=-5,7,-11,13} \frac{k_{hi}s}{s^2 + (\omega_0 h)^2} \tag{39}$$

where $k_{pv}$ and $k_{pi}$ are the proportional coefficients, $k_{rv}$ and $k_{ri}$ are the resonant coefficients at the fundamental frequency, $k_{hv}$ and $k_{hi}$ represent the voltage and current resonant controller coefficients for the $h^{th}$ order harmonic component.

The total output impedance with the virtual impedance loop can be derived as

$$Z_{C\alpha\beta}(s) = G(s)(Z_{v\alpha\beta,f}^{+}(s) + Z_{v\alpha\beta,h}(s)) + Z_{o\alpha\beta}(s) \tag{40}$$

From (35)-(40), the equivalent impedance model of a DG unit can be derived, as shown in Fig. 9(b).
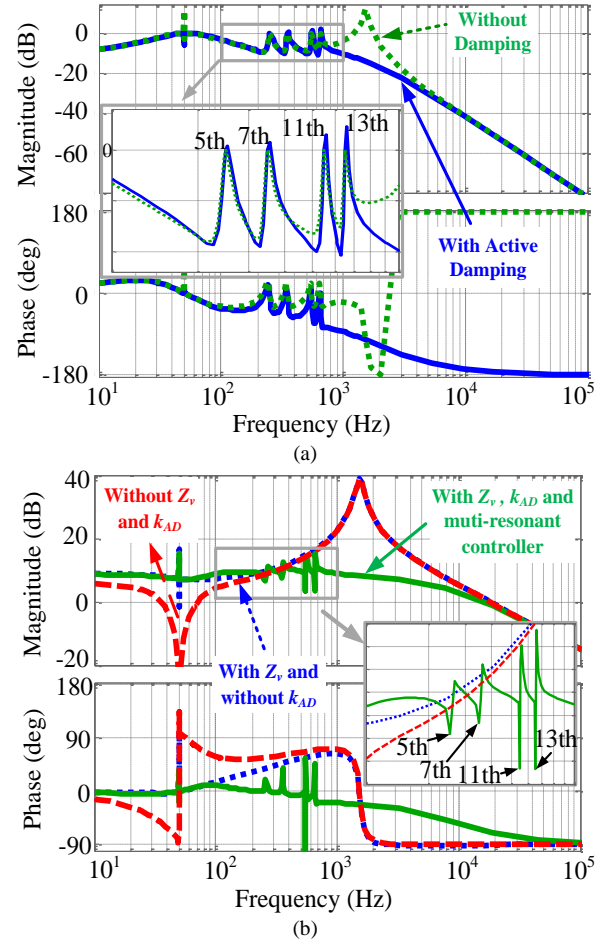


Fig. 10. Bode plots of the closed-loop voltage gain and the output impedance of a DG unit. (a) Closed-loop voltage gain of $G(s)$ with PR plus multi-resonant controller. (b) The output impedance with PR and multi-resonant controllers.

By using the closed-loop model described by (35)-(40), the bode plots of the closed-loop voltage gain and the output impedance with and without AD method are illustrated in Fig. 10. From Fig. 10(a), it can be observed that the AD method ensures effective damping at LCL resonance frequency and the system shows sufficient stability margin. The gains of the closed-loop voltage controller are unity at the fundamental and $5^{th}$, $7^{th}$, $11^{th}$, and $13^{th}$ harmonic frequencies, respectively, which means the system obtains the zero-error tracking capability at both the fundamental frequency and target characteristic harmonic frequencies.

The total output impedance $Z_{C\alpha\beta}(s)$ of a DG unit under PR controller plus virtual impedance loops which contains the virtual positive- and negative-sequence impedance, and the virtual variable harmonic impedance loops without AD is given in Fig. 10(b). It shows that, the total output impedance is about 40 dB without AD under resonance frequency of the LC filter and about 20 dB under the considered frequencies such as $-5f_0$, $7f_0$, $-11f_0$, $13f_0$, etc. Large output impedance leads to a large harmonic voltage drop under current harmonics, which distorts the output voltage [7]. The total output impedance of the DG under PR plus multi-resonant controller with virtual impedance loops using AD method, $Z_{C\alpha\beta}(s)$ is greatly reduced and lower voltage distortion can be expected under nonlinear loads.

## III. EXPERIMENTAL RESULTS

In order to validate the feasibility of the proposed enhanced hierarchical control strategy, the experimental results obtained from two paralleled-connected DG units are presented and compared. The experimental setup was built and tested in the Microgrid Research Lab of Aalborg University [32], which consists of two 2.2kW Danfoss inverters connected in parallel with linear and nonlinear loads, and dSPACE1106 platform was used to implement the control algorithms. The controller parameters of the MG are shown in Table I and II. The schematic and photo of experimental setup are shown in Fig.11 and Fig.12, respectively.

TABLE II
SYSTEM PARAMETERS OF EXPERIMENTAL SETUP

| Symbol | Parameter | Value |
|---|---|---|
| $v_{dc}, v_{MG}$ | DC and MG voltages | 650 V, 311 V |
| $f_0, f_s$ | MG and switching frequencies | 50 Hz, 10 kHz |
| $L, L_o$ | Filter and output inductances | 1.8 mH, 1.8 mH |
| $C$ | Filter capacitor | 25 μF |
| $R_L$ | Balanced resistive load | 115/230 Ω |
| $L_{NL}, R_{NL}, C_{NL}$ | Nonlinear load | 84 μH, 460 Ω, 235 μF |
| $k_{AD}$ | Active damping coefficient | 28.5 |
| $k_{pv}, k_{rv}, k_{5,7,11,13v}$ | Voltage loop PR parameters | 0.175, 200, 50, 40, 20, 20 |
| $k_{pi}, k_{ri}, k_{5,7,11,13i}$ | Current loop PR parameters | 3, 50, 10, 10, 5, 5 |
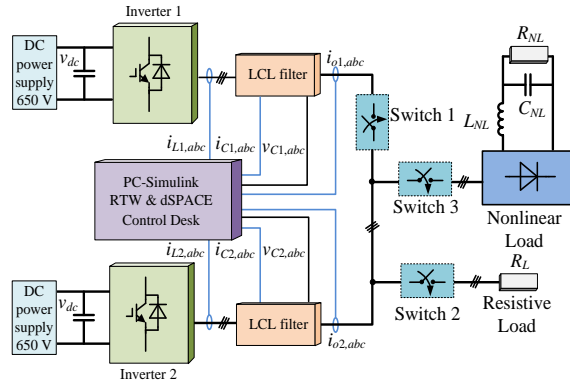


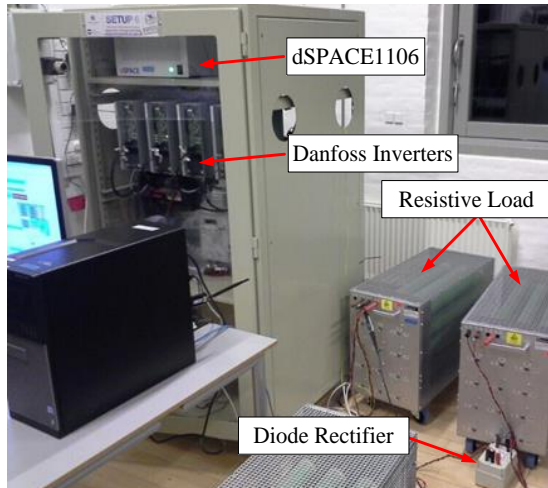Fig. 11. Schematic of the experimental setup using parallel DG units.



Fig. 12 Photo of the experimental setup.

The experimental results of the VSIs in the islanded MG system with and without using the proposed virtual impedance loops and AD method under resistive load conditions are compared in Fig. 13 and Fig. 14. As shown in Fig. 13, small output voltages of inverter 1 and inverter 2 would result in severe output currents oscillations, and higher output voltages reference would trip the converters due to the overcurrent protection. Fig. 14 shows the experimental results of the MG under resistive load conditions, when the inner loop AD scheme with $k_{AD}$=28.5 and the proposed virtual impedance loops with the virtual positive- and negative-sequence impedance, and the virtual variable harmonic impedance loops are used. It is observed that the oscillations of the output currents are alleviated with the proposed AD method and virtual impedance loops, which confirms theoretical analysis.



(a)

(b)

(c)

(d)

Fig. 13. Experimental results of the islanded MG system without using the proposed control method under resistive load conditions. (a) The output voltages of inverter 1. (b) The output currents of inverter 1. (c) The output voltages of inverter 2. (d) The output currents of inverter 2.
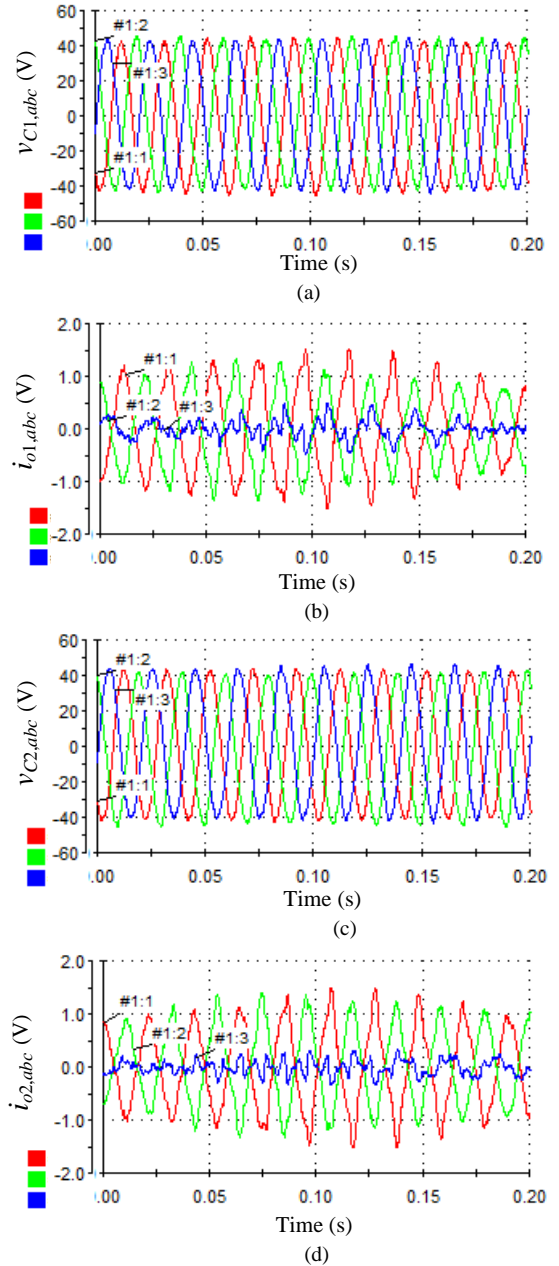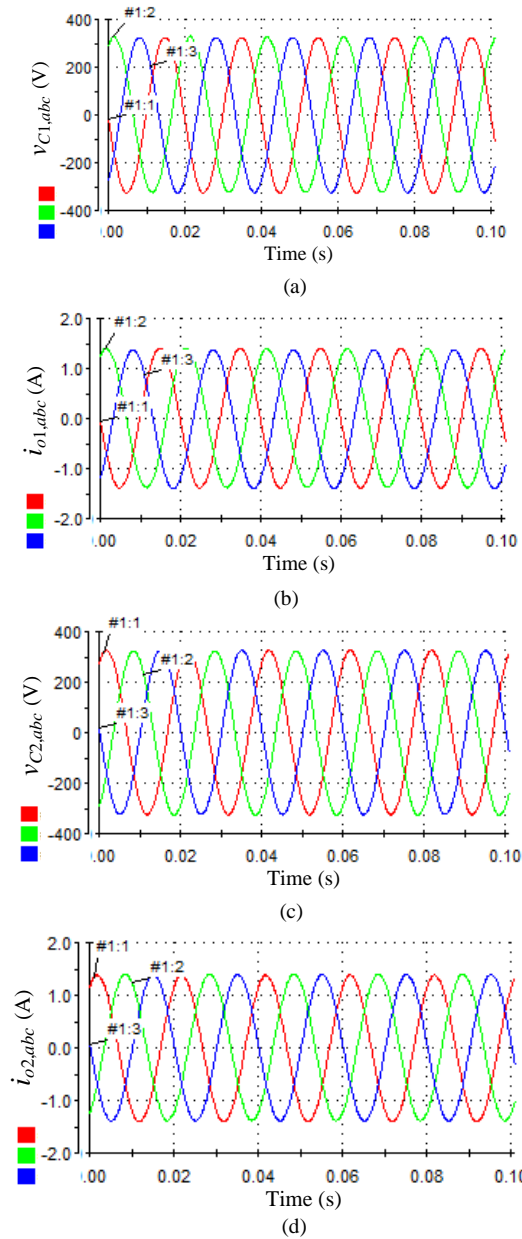
(a)



(b)



(c)



(d)

Fig. 14. Experimental results of the islanded MG system with using the proposed control method under resistive load conditions. (a) The output voltages of inverter 1. (b) The output currents of inverter 1. (c) The output voltages of inverter 2. (d) The output currents of inverter 2.
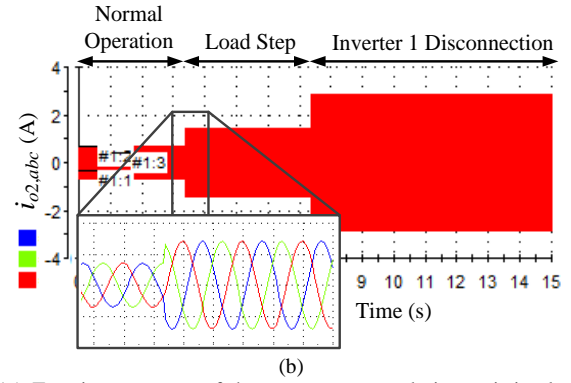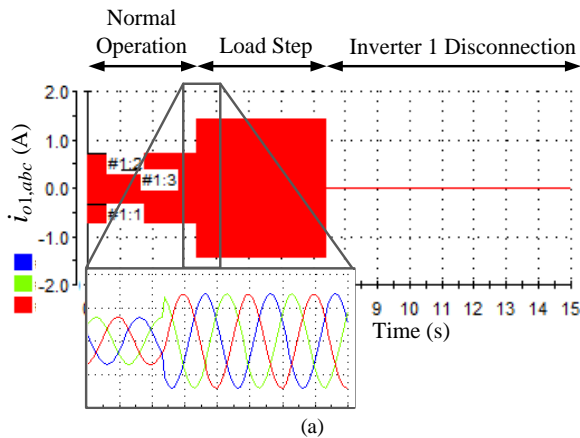


(a)



(b)

Fig. 15. Transient response of the output currents during resistive load step changes ($t$=3.53s) and sudden disconnection of inverter 1 ($t$=7.35s). (a) The output currents of inverter 1. (b) The output currents of inverter 2.

Fig. 15 shows the output currrent waveforms of the MG sharing the resistive load by using the droop method with the additional phase-shift loop ($k_d$) and AD ($k_{AD}$) method. Both inverters are sharing the resistive load in the normal operation mode, and a load step increase of 230 $\Omega$ is suddenly applied at $t$=3.35 s and inverter 1 is disconnected at $t$=7.35 s, while only inverter 2 is supplying the total load currents. As shown in Fig. 15, the inverter 2 can supply the load and the system remains stable when inverter 1 trips.
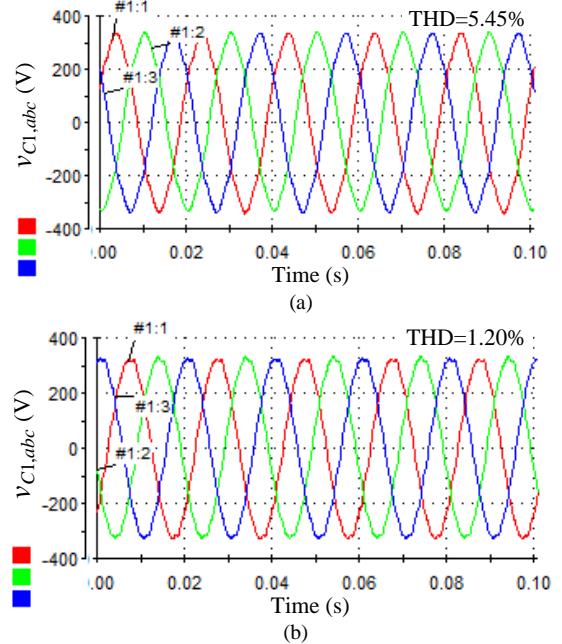


(a)



(b)

Fig. 16. Experimental results of the output voltages of a VSI. (a) The output voltages of inverter 1 without using the proposed method. (b) The output voltages of inverter 1 with using the proposed method.

Fig.16 shows a comparison of the experimental results of the islanded MG system under nonlinear load conditions with and without using the virtual impedance loops which contains the virtual positive- and negative-sequence impedance, and the virtual variable harmonic impedance loops and harmonic compensation in the voltage and current loops. As shown in Fig. 16(a), when the harmonic compensation is not activated and only the virtual positive- and negative-sequence impedance loops are activated, the output voltages are severely distorted by nonlinear loads and the total harmonic distortion (THD) of output voltage is about 5.45%. Fig. 16(b) shows the

experimental results when harmonic compensation is enabled and the proposed control method is used, where the multiple PR controllers are tuned at the $5^{th}$, $7^{th}$, $11^{th}$, and $13^{th}$ harmonic frequencies in the voltage and current loops. In this case, THD of output voltage is reduced to 1.20%. It can be concluded that the THDs of the output voltages are effectively reduced with the proposed control strategies which contains AD method, harmonic compensation and the virtual positive- and negative-sequence impedance, and the virtual variable harmonic impedance loops.
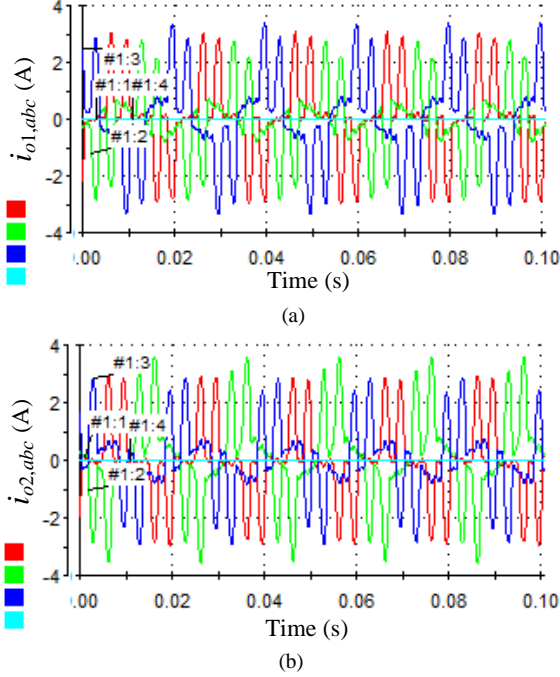


(a)



(b)

Fig. 17. Experimental results of the islanded MG system with the conventional droop control. (a) The output currents of inverter 1. (b) The output currents of inverter 2.

Fig. 17 shows the performance of the MG when the control of the virtual positive- and negative-sequence impedance, and the virtual variable harmonic impedance loops are not activated. It is shown that the currents of inverter 1 and 2 are not identical, due to the circulating currents between these DG units. When the power sharing errors are compensated by using the proposed method, the transient response of the currents under nonlinear loads are given in Fig. 18. From Fig. 17 and Fig. 18, it is shown that the current sharing errors are effectively reduced and inverter 1 and 2 have similar output currents and the reactive and harmonic power sharing performances are improved. Note that the virtual harmonic impedance at the dominant harmonic frequencies, i.e., $5^{th}$, $7^{th}$, $11^{th}$, and $13^{th}$ are controlled. The higher harmonic frequencies can also be controlled in the virtual variable harmonic impedance loop when needed. The stability of the MG is also guaranteed under nonlinear load conditions when the load step and sudden disconnection of one DG unit are applied.

The experimental results of the islanded MG system with and without using the secondary controller for the proposed control scheme under resistive load conditions are shown in Fig. 19. Fig. 19(a)~(c) show the experimental results without using the secondary controller and when a load change is suddenly applied at $t$=3.35 s and the first inverter is disconnected at

$t$=7.35 s. As shown in Fig. 19(a), the active power ($P_1$, $P_2$) and reactive power ($Q_1$, $Q_2$) sharings of the two DG units are achieved. And small amount of reactive power can be observed due to the effect of output inductance ($L_o$).
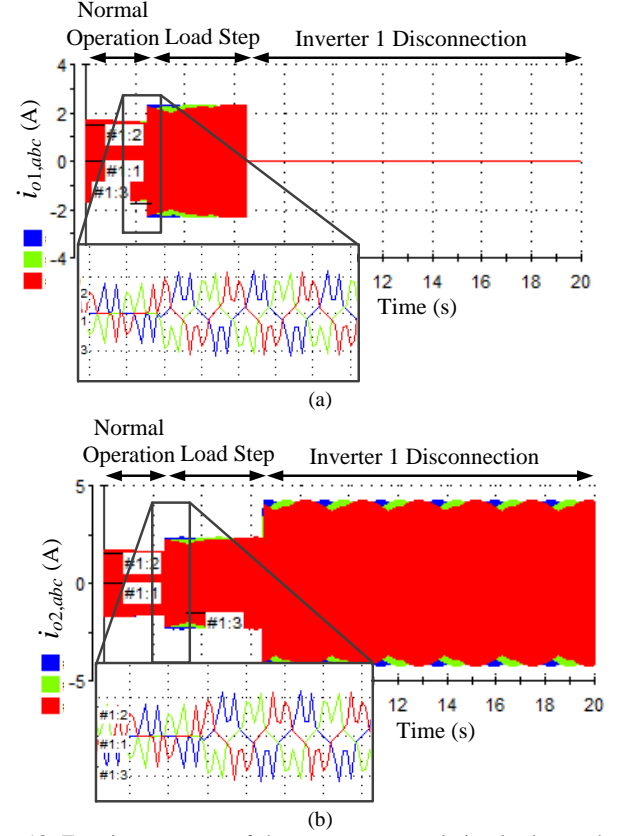


(a)



(b)

Fig. 18. Transient response of the output currents during load step changes ($t$=3.53s) and sudden disconnection of inverter 1 ($t$=7.35s) under nonlinear loads with the proposed virtual impedance loop and harmonic compensation controls. (a) The output currents of inverter 1. (b) The output currents of inverter 2.

As depicted in Fig. 19(b), the peak voltages of inverter 1 and 2 are not exactly the same under normal operation conditions, and small deviation is observed. With an increase of the load is applied at $t$=3.35 s, the peak voltage of inverter 2 drops and the voltage of inverter 1 increases. When inverter 1 is swithed off at $t$=7.35 s, the peak voltage of inverter 2 drops again due an increase of load. As shown in Fig. 19(c), the frequency is deviated from 50Hz, i.e., a steady-state error about 0.005Hz can be observed under normal operation conditions. With an increase of load, the frequencies of both inverter 1 and inverter 2 drop for about 0.006 Hz. After the tripping of inverter 1, the frequency of the MG drops for 0.01Hz to reach a steady state of 49.976 Hz.

Fig. 19(d)~(f) show the performance of the islanded MG with using the secondary controller. Fig. 19(d) shows the dynamic response of the active power and reactive power in the DGs for each scenario. Note that there is a small increase in active power to restore the frequency deviation when the secondary control is activated.

The effect of the secondary control strategy to restore voltage and frequency deviations of the DGs are depicted in Fig. 19(e) and (f). Notice that the deviations in voltage amplitude and frequency due to droop control and virtual impedance loops are recovered to the nominal values. Fig. 19(e) shows the peak

Fig. 19. Performance of the islanded MG consists of two DGs without (a~c) and with (d~e) using secondary controller under the resistive load conditions. (a) and (d) Active and reactive powers. (b) and (e) Voltage amplitude. (c) and (f) Frequency.
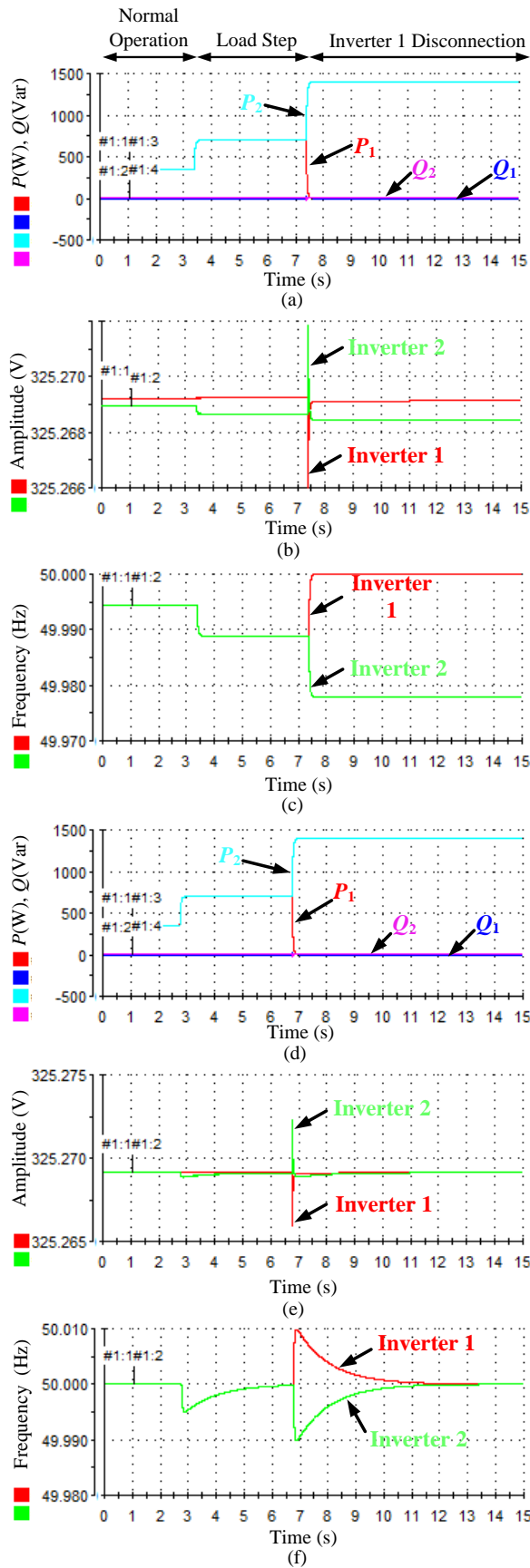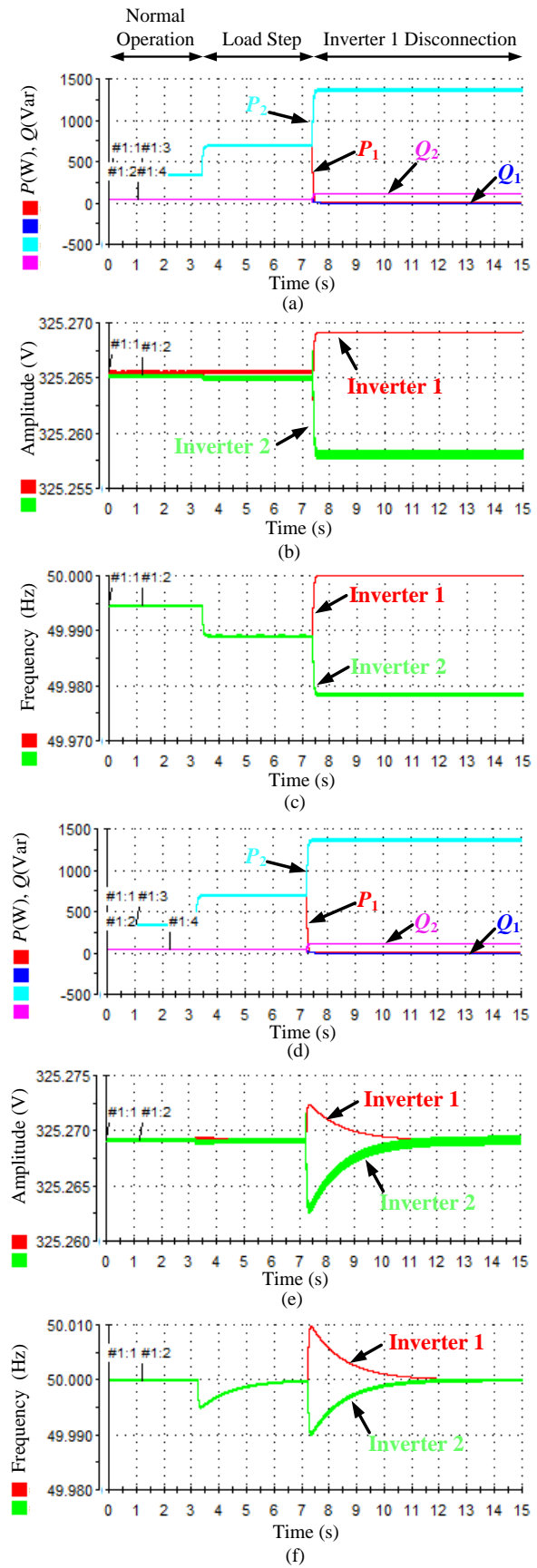


Fig. 20. Performance of the islanded MG consists of two DGs without (a~c) and with (d~e) using secondary controller under the nonlinear load conditions. (a) and (d) Active and reactive powers. (b) and (e) Voltage amplitude. (c) and (f) Frequency.

voltages of inverter 1 and 2 are identical under the normal operation scenario. The voltage amplitude restoration can be observed when a sudden increase of load is applied, and voltage amplitude recovers to the nominal value successfully even after disconnection of the inverter 1. Fig. 19(f) shows that the frequencies of inverter 1 and 2 are controlled to 50 Hz simultaneously under normal operation conditions. When the loads are suddenly increased, both frequency curves drop and gradually recover to 50 Hz. In the last scenario, the frequency restoration of inverter 2 is also achieved when the inverter 1 is switched off from the MG at $t$=6.8 s, which recovers to the pre-defined frequency after a few seconds.

Fig. 20 shows the experimental results of the islanded MG system for the proposed control scheme under nonlinear load conditions. Fig. 20(a)~(c) show the performance of the MG without using secondary controller and when a balanced resistive load is suddenly applied at $t$=3.35 s and inverter 1 is disconnected at $t$=7.35 s. And Fig. 20(d)~(f) show the performance of the islanded MG with using the secondary controller, respectively.

Fig. 20(a) and (d) show that the active powers and reactive powers can be shared between DGs by means of droop control and enhanced virtual impedance loop, no matter with or without using the secondary control. These results illustrates that the $P$-$\omega$ droop control is sufficient to share the active power once the virtual impedance loops and inner AD scheme are adopted, since the frequency is a global variable in the MG system [5]. The proposed secondary control is able to keep the reactive power shared between DG units under load variations. After disconnection of the inverter 1 from the MG system in the last scenario, inverter 2 feeds the load currents by injecting the doubled active power. By comparing Fig. 20(b), (c) and (e), (f), it can be observed that frequency and voltage amplitude restoration of the DG units can be achieved by means of the secondary control strategy.

## IV. Conclusion

This paper presents an enhanced hierarchical control for 3-phase parallel-connected VSI-based islanded MGs. The proposed method utilizes the primary control which is based on the virtual impedance loops with the virtual positive- and negative-sequence impedance loops at fundamental frequency, and the virtual variable harmonic impedance loop at harmonic frequencies, and droop control scheme with an additional phase-shift loop to enhance the sharing of reactive power and harmonic power between the DG units. The moving average filter-based sequence decomposition has been proposed to accurately extract the fundamental positive and negative sequences, and harmonic components for the virtual impedance loops. With the centralized controller of the secondary control, the voltage amplitude and frequency restoration are achieved. The developed small-signal model for the primary and secondary controls shows that, an overdamped feature of the power loop is achieved to improve the whole MG system damping.

A multi-loop control strategy with the inner-loop AD method for resistive and nonlinear load conditions is also presented. The capacitor currents of the LCL filter are used as feedback signals to actively damp the high frequency resonances while an outer voltage loop with output virtual impedance regulates the output voltage and ensure system stability over a wide range of operating conditions. Experimental results from two parallel-connected DG units verified the effectiveness of the proposed control strategies.

## References

[1] R. J. Wai, C. Y. Lin, Y. C. Huang, and Y. R. Chang, "Design of high performance stand-alone and grid-connected inverter for distributed generation applications," *IEEE Trans. Ind. Electron.*, vol. 60, no. 4, pp. 1542-1555, Apr. 2013.

[2] D. E. Olivares, A. Mehrizi-Sani, A. H. Etemadi, C. A. Canizares, R. Iravani, and M. Kazerani, "Trends in microgrids control," *IEEE Trans. Smart Grid.*, vol. 5, no. 4, pp. 1905-1919, Jul. 2014..

[3] X. Tang, X. Hu, N. Li, W. Deng, and G. Zhang, "A novel frequency and voltage control method for islanded microgrid based on multienergy storages," *IEEE Trans. Smart Grid.*, vol. pp, no. 99, 2014. 10.1109/TSG.2014.2381235.

[4] M. A. Mahmud, M. J. Hossain, H. R. Pota, and A. M. T. Oo, "Robust nonlinear distributed controller design for active and reactive power sharing in islanded microgrids," *IEEE Trans. Energy Covers.*, vol. 29, no. 4, pp. 893-903, Dec. 2014.

[5] Q. Shafiee, J. M. Guerrero, and J. C. Vasquez, "Distributed secondary control for islanded microgrids-A novel approach," *IEEE Trans. Power Electron.*, vol. 29, no. 2, pp. 1018-1031, Feb. 2014.

[6] H. Xin, L. Zhang, D. Gan, and K. P. Wong, "Control of island AC microgrids using a fully distributed approach," *IEEE Trans. Smart Grid.*, vol. 6, no. 2, pp. 943–945, Mar. 2015.

[7] Q. Liu, Y. Tao, X. Liu, Y. Deng, and X. He, "Voltage unbalance and harmonics compensation for islanded microgrid inverters," *IET Power Electron.*, vol. 7, no. 5, pp. 1055–1063, May. 2014.

[8] H. J. Avelar, W. A. Parreira, J. B. Vieira, L. C. G. de Freitas, and E. A. Alves Coelho, "A state equation model of a single-phase grid-connected inverter using a droop control scheme with extra phase shift control action," *IEEE Trans. Ind. Electron.*, vol. 59, no. 3, pp. 1527-1537, Mar. 2012.

[9] M. Savaghebi, A. Jalilian, J. C. Vasquez, and J. M. Guerrero, "Secondary control scheme for voltage unbalance compensation in an islanded droop-controlled microgrid," *IEEE Trans. Smart Grid.*, vol. 3, no. 2, pp. 797-807, Jun. 2012.

[10] P. Arboleya, C. Gonzalez-Moran, M. Coto, M. C. Falvo, L. Martirano, and D. Sbordone, "Efficient energy management in smart Micro-grids: zero grid impact buildings," *IEEE Trans. Smart Grid.*, vol. 6, no. 2, pp. 1055-1063, Mar. 2015.

[11] A. Bidram, and A. Davoudi, "Hierarchical structure of microgrids control system," *IEEE Trans. Smart Grid.*, vol. 3, no. 4, pp. 1963-1976, Dec. 2012.

[12] M. Rasheduzzaman, J. Mueller, and J. Kimball, "An accurate small-signal model of inverter-dominated islanded microgrids using dq reference frame," *IEEE Trans. Power Electron.*, vol. 2, no. 4, pp. 1070-1080, Dec. 2014.

[13] Y. Tao, Q. Liu, Y. Deng, X. Liu, and X. He, "Analysis and mitigation of inverter output impedance impacts for distributed energy resource interface," *IEEE Trans. Power Electron.*, vol. 30, no. 7, pp. 3563-3576, Jul. 2015.

[14] J. He, and Y. W.Li, "Analysis, design, and implementation of virtual impedance for power electronics interfaced distributed generation," *IEEE Trans. Ind. Appl.*, vol. 47, no. 6, pp. 2525-2538, Nov./Dec. 2011.

[15] X. Lu, J. M. Guerrero, K. Sun, J. C. Vasquez, R. Teodorescu, and L. Hua, "Hierarchical control of parallel ac-dc converter interfaces for hybrid microgrids," *IEEE Trans. Smart Grid.*, vol. 5, no. 2, pp. 683-692, Mar. 2014.

[16] *IEEE Recommended Practices and Requirements for Harmonic Control in Electrical Power System*, IEEE Std. 519, 1992.

[17] J. He, Y. W. Li, R. Wang, and C. Zhang, "Analysis and mitigation of resonance propagation in grid-connected and islanding microgrids," *IEEE Trans. Energy Covers.*, vol. 30, no. 1, pp. 70-81, Mar. 2015.

[18] R. Pena-Alzola, M. Liserre, F. Blaabjerg, R. Sebastian, J. Dannehl, and F. W. Fuchs, "Analysis of the passive damping losses in LCL-filter-based grid converters," *IEEE Trans. Power Electron.*, vol. 28, no. 6, pp. 2642-2646, Jun. 2013.

[19] J. Dannehl, M. Liserre, and F. W. Fuchs, "Filter-based active damping of voltage source converters with *LCL*-filter," *IEEE Trans. Ind. Electron.*, vol. 58, no. 8, pp. 3623-3633, Aug. 2011.

[20] J. Xu, S. Xie, and T. Tang, "Active damping-based control for grid-connected LCL-filtered inverter with injected grid current feedback only," *IEEE Trans. Ind. Electron.*, vol. 61, no. 9, pp. 4746-4758, Sep. 2014.

[21] X. Lu, J. M. Guerrero, R. Teodorescu, T. Kerekes, K. Sun, and L. Huang, "Control of parallel-connected bidirectional AC-DC converters in stationary frame for microgrid application," in *proc*. *IEEE ECCE*, 2011, vol. 5, pp. 4153-4160.

[22] M. Savaghebi, M. M. Hashempour, and J. M. Guerrero, "Hierarchical coordinated control of distributed generators and active power filters to enhance power quality of microgrids," in *proc*. *IEEE RTUCON*, 2014, pp. 259-264.

[23] D. Wu, F. Tang, T. Dragicevic, J. C. Vasquez, and J. M. Guerrero, "Autonomous active power control for islanded ac microgrids with photovoltaic generation and energy storage system," *IEEE Trans. Energy Convers.*, vol. 29, no. 4, pp. 882-892, Dec. 2014.

[24] J. M. Guerrero, J. C. Vasquez, J. Matas, M. Castilla, L. G. D. Vicua, and M. Castilla, "Hierarchical control of droop-controlled AC and DC microgrids—A general approach toward standardization," *IEEE Trans. Ind. Electron.*, vol. 58, no. 1, pp. 158–172, Jan. 2011.

[25] J. M. Guerrero, P. Loh, M. Chandorkar, and T. Lee, "Advanced control architectures for intelligent microgrids—Part I: Decentralized and hierarchical control," *IEEE Trans. Ind. Electron.*, vol. 60, no. 4, pp. 1263–1270, Apr. 2013.

[26] J. Vasquez, J. M. Guerrero, M. Savaghebi, J. Eloy-Garcia, and R. Teodorescu, "Modeling, analysis, and design of stationary reference frame droop controlled parallel three-phase voltage source inverters," *IEEE Trans. Ind. Electron.*, vol. 60, no. 4, pp. 1271–1280, Apr. 2013.

[27] X. Wang, F. Blaabjerg, and Z. Chen, "Autonomous control of inverter-interfaced distributed generation units for harmonic current filtering and resonance damping in an islanded microgrid," *IEEE Trans. Ind. Appl.*, vol. 50, no. 1, pp. 452-461, Jan/Feb. 2014.

[28] S. Golestan, M. Ramezani, J. M. Guerrero, F. D. Freijedo, and M. Monfared, "Moving average filter based phase-locked loops: performance analysis and design guidelines," *IEEE Trans. Power Electron.*, vol. 29, no. 6, pp. 2750-2763, Jun. 2014.

[29] H. Mahmood, D. Michaelson, and J. Jiang, "Accurate reactive power sharing in an islanded microgrid using adaptive virtual impedances," *IEEE Trans. Power Electron.*, vol. 30, no. 3, pp. 1605-1617, Mar. 2015.

[30] J. He and Y. W. Li, "Analysis, design, and implementation of virtual impedance for power electronics interfaced distributed generation," *IEEE Trans. Ind. Appl.*, vol. 47, no. 6, pp. 2525-2538, Nov./Dec. 2011.

[31] T. Lee, and P. T. Cheng, "Design of a new cooperative harmonic filtering strategy for distributed generation interface converters in an islanding network," *IEEE Trans. Power Electron.*, vol. 22, no. 5, pp. 1919-1927, Sep. 2007.

[32] Microgrid Research Programme, Aalborg University: www.microgrids.et.aau.dk.

**Pan Shen** was born in Hefei, China in 1991. He received his B.S. in Electrical Engineering and Automation from Anhui Agricultural University, Hefei, China, in 2013. He is currently working toward the M.S. degree in Power Electronics and Electric Drives at the University of Electronic Science and Technology of China (UESTC), Chengdu, China. His current research interests include ac/dc microgrid, power quality, power converters, power system automation, and active power filters.

**Xin Zhao** received the B.S. and M.S. degree in Power Electronics & Electrical Drives from Northwestern Polytechnical University, Xi'an, China, in 2010 and 2013, respectively. He is currently working toward the Ph.D. degree at Department of Energy Technology, Aalborg University, Denmark. His research interests include control of power converters, power quality and microgrids.

**Josep M. Guerrero** (S'01-M'04-SM'08-FM'15) received the B.S. degree in telecommunications engineering, the M.S. degree in electronics engineering, and the Ph.D. degree in power electronics from the Technical University of Catalonia, Barcelona, in 1997, 2000 and 2003, respectively. Since 2011, he has been a Full Professor with the Department of Energy Technology, Aalborg University, Denmark, where he is responsible for the Microgrid Research Program. From 2012 he is a guest Professor at the Chinese Academy of Science and the Nanjing University of Aeronautics and Astronautics; from 2014 he is chair Professor in Shandong University; and from 2015 he is a distinguished guest Professor in Hunan University.

His research interests is oriented to different microgrid aspects, including power electronics, distributed energy-storage systems, hierarchical and cooperative control, energy management systems, and optimization of microgrids and islanded minigrids. He is an Associate Editor for the IEEE TRANSACTIONS ON POWER ELECTRONICS, the IEEE TRANSACTIONS ON INDUSTRIAL ELECTRONICS, and the IEEE Industrial Electronics Magazine, and an Editor for the IEEE TRANSACTIONS on SMART GRID and IEEE TRANSACTIONS on ENERGY CONVERSION. He has been Guest Editor of the IEEE TRANSACTIONS ON POWER ELECTRONICS Special Issues: Power Electronics for Wind Energy Conversion and Power Electronics for Microgrids; the IEEE TRANSACTIONS ON INDUSTRIAL ELECTRONICS Special Sections: Uninterruptible Power Supplies systems, Renewable Energy Systems, Distributed Generation and Microgrids, and Industrial Applications and Implementation Issues of the Kalman Filter; and the IEEE TRANSACTIONS on SMART GRID Special Issue on Smart DC Distribution Systems. He was the chair of the Renewable Energy Systems Technical Committee of the IEEE Industrial Electronics Society. In 2014 he was awarded by Thomson Reuters as Highly Cited Researcher, and in 2015 he was elevated as IEEE Fellow for his contributions on "distributed power systems and microgrids."

**Yang Han** (S'08-M'10) was born in Chengdu, China. He received his Ph.D. in Electrical Engineering from Shanghai Jiaotong University (SJTU), Shanghai, China, in 2010. He joined the Department of Power Electronics, School of Mechatronics Engineering, University of Electronic Science and Technology of China (UESTC) in 2010, and where he has been an Associate Professor since 2013. From March 2014 to March 2015, he was a Visiting Scholar at the Department of Energy Technology, Aalborg University, Aalborg, Denmark. His research interests include AC/DC microgrids, grid-connected converters for renewable and DGs, phase-locked loop (PLL), power quality, active power filters and static synchronous compensators (STATCOMs). He has authored more than 20 ISI-indexed journal papers in the area of power electronics, power quality conditioners, and smart grid. He received Best Paper Awards from 2013 Annual Conference of HVDC and Power Electronics Committee of Chinese Society of Electrical Engineers (CSEE) in Chongqing, China, and the 4th International Conference on Power Quality in 2008, in Yangzhou, China.